Real-time Factor Graph Optimization Aided by Graduated Non-convexity Based Outlier Mitigation for Smartphone Decimeter Challenge

Yihan Zhong, Weisong Wen, Hoi-Fung Ng, Xiwei Bai, Li-Ta Hsu
Department of Aeronautical and Aviation Engineering, The Hong Kong Polytechnic University

BIOGRAPHY

Mr.Zhong obtained his bachelor's degree in process equipment and control engineering from Guangxi University in 2020 and a Master's degree from The Hong Kong Polytechnic University (PolyU). He is currently a Ph.D. student at the Department of Aeronautical and Aviation Engineering (AAE) of PolyU. His research interests include factor graph optimization-based collaborative positioning and low-cost localization.

Weisong Wen received a Ph.D. degree in Mechanical Engineering from The Hong Kong Polytechnic University (PolyU), in Nov 2020. He was also a visiting Ph.D. student with the Faculty of Engineering, University of California, Berkeley (UC Berkeley) in 2018. In 2020, he won the Best Presentation Award from the Institute of Navigation (ION), and the First Prize in Hong Kong Section in Qianhai-Guangdong-Macao Youth Innovation and Entrepreneurship Competition, 2019. Before joining PolyU as a Research Assistant Professor in April 2021, he was a senior research fellow at PolyU. His research interests include GNSS positioning, SLAM, and collaborative positioning in challenging environments autonomous driving vehicles, and unmanned aerial vehicles.

Li-Ta Hsu received B.S. and Ph.D. degrees in aeronautics and astronautics from National Cheng Kung University, Taiwan, in 2007 and 2013, respectively. He is currently an assistant professor with the Interdisciplinary Division of Aeronautical and Aviation Engineering, The Hong Kong Polytechnic University, before he served as a post-doctoral researcher in the Institute of Industrial Science at the University of Tokyo, Japan. In 2012, he was a visiting scholar at University College London, the U.K. His research interests include GNSS positioning in challenging environments and localization for pedestrians, autonomous driving vehicle, and unmanned aerial vehicle

ABSTRACT

Real-time reliable navigation in urban environments has received academic and commercial interest over recent years. Unfortunately, commercial sensors such as smartphones are implemented with low-cost antennas and chips for receiving satellite signals and suffered from severe signal degrading caused by the non-light-of-sight (NLOS) and multi-path effect. Many conventional methods like extended Kalman filter (EKF) would always perform poorly in the urban environment. Factor graph optimization (FGO) has recently proved its reliable navigation performance in urban environments, utilizing the multi-epoch GNSS measurements to estimate the user position simultaneously. Furthermore, recent studies verified that outlier mitigation technologies using graduated non-convexity (GNC) could effectively improve GNSS positioning performance. However, those studies are mainly concerned with batch optimization which makes the computational load significant and leads to large time consumption, especially while the system integrates the GNC-based robust function in optimization for outlier mitigation. For smartphones application, this study proposed a real-time sliding window-based FGO with the implementation of GNC for outlier mitigation to guarantee reliability and low time consumption. This paper verifies the effectiveness of the contributions of this paper step by step using datasets in Shang Hai and Los Angeles. We also discussed the impact of the different sizes of sliding windows in terms of positioning error and time consumption.

1. INTRODUCTION

Smartphones are pervasive today and have become one of the most popular commercial devices for users in urban environments, especially after the Google team released that the smartphone application had access to the raw GNSS measurements in 2016. Nevertheless, smartphone GNSS positioning in urban canyons is still challenging due to the non-line-sight and multi-path effect. To raise awareness of smartphone urban positioning, the Android team of Google held a Smartphone Decimeter Challenge in conjunction with ION GNSS+ 2021[1]. Lots of methods[2, 3] are developed to compete for the best smartphone positioning

accuracy. Among all these methods, the winner, Dr. Taro Suzuki, disclosed his algorithm at the conference [1]. Interestingly, the challenge winner utilizes the recent popular framework factor graph optimization (FGO) to achieve good performance [4]. Specifically, the GNSS pseudorange and time-differenced carrier-phase measurements are structured into a factor graph model which is then further optimized to get the trajectory of the smartphone. With the help of the FGO, the time correlation between the historical measurements can be exploited to improve the system's robustness. Moreover, Dr. Taro Suzuki adopted the switchable constraints [5] to model the possible existence of the GNSS outlier measurements, such as the multi-path and NLOS receptions. Applying the FGO attracts lots of attention [6-9]. Also, there is a review of recent work on FGO [10]. This review precisely figured out that the FGO is not a new method but a framework and concisely introduced the FGO history in GNSS positioning.

Previously, to investigate the potential of FGO in GNSS standalone positioning, we developed the FGO-based open-source framework for GNSS positioning considering the pseudorange, Doppler, and carrier-phase measurements [11]. Improved positioning result was achieved compared with the conventional extended Kalman filter (EKF) based solution. Moreover, our previous work in [9] theoretically and experimentally compared the EKF and the FGO -based GNSS pseudorange and inertial measurement unit (IMU) integration, and similar findings were obtained. In short, the FGO in GNSS positioning obtains improved accuracy compared with the EKF-based solution. Although the advantage of the FGO, the switchable constraints [5] used by Dr. Taro Suzuki in the last Smartphone Decimeter Challenge can not fully mitigate the impacts of the GNSS outlier measurements and the smartphone positioning accuracy still have lots of room to improve. The Massachusetts Institute of Technology team recently proposed a graduated non-convexity (GNC) aided robust and global outlier rejection for point cloud registration [12]. However, they solely consider the measurements of every single epoch. To mitigate the outliers of GNSS measurements, we proposed a method combining FGO and GNC and prove its robustness and accuracy in several challenging datasets of Hong Kong [13]. Unfortunately, utilizing GNC would cause a high computational load and lead to a large time consumption which is unacceptable for a smartphone.

To achieve robust real-time estimation for urban navigation and inspired by the previous work, this paper proposes to decrease the time consumption of the estimation for real-time application scenarios. Firstly, we extend the previous batch method to the sliding window-based optimization to decrease the computational load by reducing the redundancy of measurements. Secondly, different from the previous loosely-coupled Doppler measurement, we use tightly-coupled Doppler for receiver velocity estimation. Finally, we use a constant velocity model that replaced the Doppler velocity factor to connect two states in the sliding window of FGO. The contributions of this paper are listed as follows:

(1) This paper proposes a sliding window-based GNSS pseudorange/ tightly-coupled Doppler integration using FGO-GNC. We extend our previous robust estimation framework to achieve real-time performance.
(2) This paper discusses the impact of the different sliding windows in terms of positioning error and time consumption.
(3) This paper verifies the effectiveness of the contributions of this paper step by step using two datasets in two cities (Shanghai and Los Angeles).

The remainder of this paper is organized as follows. An overview of the proposed method is given in Section 2. All the modeled factors in our system are given in Section 3. In Section 4, two experiments are performed to evaluate the effectiveness of the proposed method using the datasets collected in Shang Hai and Los Angeles urban canyons. The discussion about time consumption and positioning performance is given in Section 5. Finally, conclusions are drawn, and further work is presented in Section 6.

2. OVERVIEW OF THE PROPOSED METHOD

The method proposed in this paper is shown in Fig. 1. The system consists of two parts: (1) modeling the GNSS measurements and constructing the sliding window for modeled measurements. (2) the adaptive weighting estimation in FGO-GNC for outlier mitigation, including the Geman McClure relaxation and weighting estimation for each pseudorange in the sliding window. In this paper, matrices are denoted in uppercase with bold letters.

Vectors are denoted in lowercase with bold letters. Variable scalars are denoted as lowercase italic letters. Constant scalars are denoted as lowercase letters. Meanwhile, the GNSS receiver's state and the satellites' position are all expressed in the east, north, and up coordinates.

To clarify the proposed pipeline, the following major notations are defined and followed by the rest of the paper.

Table 1. Symbols and their description in this paper

Symbol	*Description*
Subscript r	the GNSS receiver
Superscript s	the index of the satellite
$\rho_{r,t}^{s}$	the pseudorange measurement received from a satellite s at a given epoch t.
$d_{r,t}^{s}$	the Doppler measurement received from satellite s at a given epoch t
$\mathbf{p}_t^s$	the position of the satellite s at a given epoch t. $\mathbf{p}_t^s = (p_{t,x}^s, p_{t,y}^s, p_{t,z}^s)^T$
$\mathbf{v}_t^s$	the velocity of the satellite s at a given epoch t. $\mathbf{v}_t^s = (v_{t,x}^s, v_{t,y}^s, v_{t,z}^s)^T$
$\mathbf{p}_{r,t}$	the position of the GNSS receiver at a given epoch t. $\mathbf{p}_{r,t} = (p_{r,t,x}, p_{r,t,y}, p_{r,t,z})^T$
$\mathbf{v}_{r,t}$	the velocity of the GNSS receiver at a given epoch t. $\mathbf{v}_{r,t} = (v_{r,t,x}, v_{r,t,y}, v_{r,t,z})^T$
$\delta_{r,t}$	the clock bias of the GNSS receiver at a given epoch t
$\delta_{r,t}^{s}$	the satellite clock bias by meters

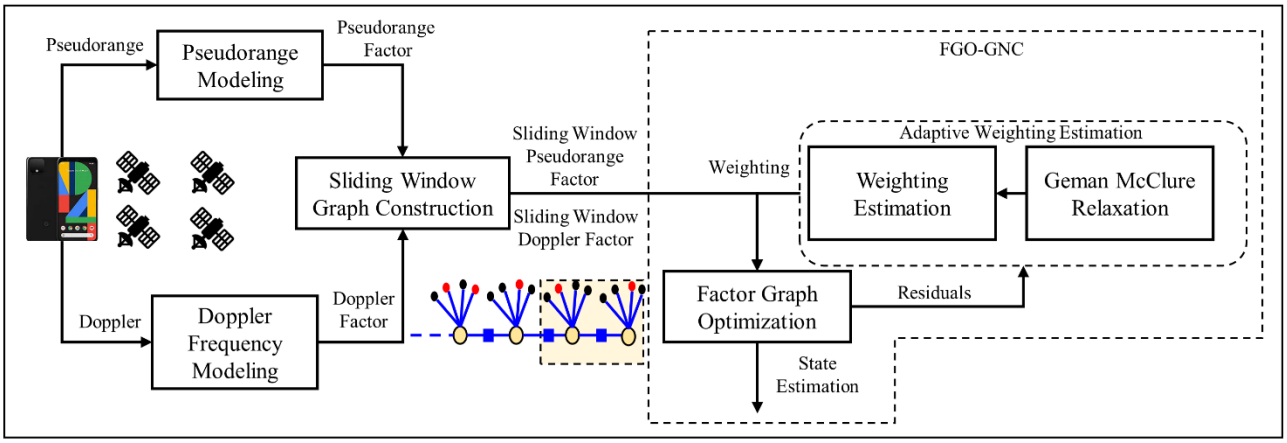

Fig. 1. Overview of the proposed method. The inputs are the raw measurements from the smartphone. The output is the state estimation of the smartphone.

3. FACTORS IN REAL-TIME FGO-GNC

This section presents the methodology for the real-time FGO-GNC system. The smartphone receives the GNSS pseudorange and Doppler measurements. Then the measurements would be modeled and transmitted into the sliding window graph construction as the factors (See Fig. 1).

The proposed factor graph for solving the GNSS positioning structure is shown in Fig.2. The subscript k denotes the total epochs of measurements considered in the real-time FGO-GNC. The smartphone state at a single epoch is represented as follows:

$$\boldsymbol{\chi} = [\mathbf{x}_{\mathrm{r},1}, \mathbf{x}_{\mathrm{r},2}, \ldots, \mathbf{x}_{r,k}] \tag{1}$$

$$\mathbf{x}_{r,t} = (\mathbf{p}_{r,t}, \mathbf{v}_{r,t}, \boldsymbol{\delta}_{r,t})^{T} \tag{2}$$

where the variable $\boldsymbol{\chi}$ denotes the set states of the GNSS receiver ranging from the first epoch to the current k. $\mathbf{x}_{r,t}$ denotes the state of the GNSS receiver at epoch t which involves the position ($\mathbf{p}_{r,t}$), velocity ($\mathbf{v}_{r,t}$) and receiver clock bias ($\boldsymbol{\delta}_{r,t}$).

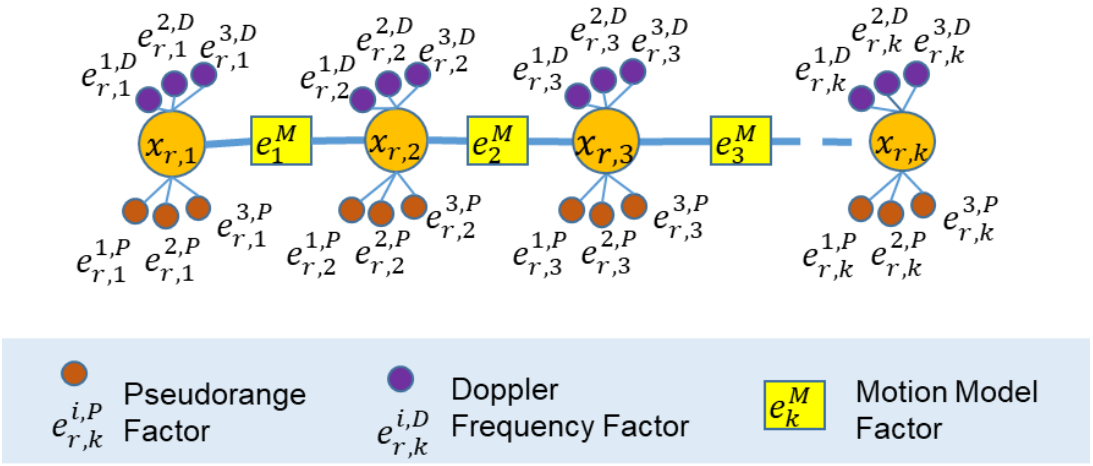

Fig. 2. Factor graph of the proposed method. The orange circles denote the states to be estimated. The purple circle is the Doppler frequency factor. The red circles represent the pseudorange factor. The yellow rectangular represents the motion model factor.

3.1 GNSS pseudorange and Doppler factor

The detailed construction of the pseudorange factor can be found in [11]. For pseudorange factors, the error function could be written as follows:

$$||\mathbf{e}_{r,t}^{s,P}||_{\mathbf{\Sigma}_{r,t}^{s}}^{2} = ||\rho_{r,t}^{s} - h_{r,t}^{s}(\mathbf{p}_{r,t}, \mathbf{p}_{t}^{s}, \delta_{r,t})||_{\mathbf{\Sigma}_{r,t}^{s}}^{2} \tag{3}$$

$$h_{r,t}^{s}(\mathbf{p}_{r,t}, \mathbf{p}_{t}^{s}, \delta_{r,t}) = ||\mathbf{p}_{t}^{s} - \mathbf{p}_{r,t}|| + \delta_{r,t} \tag{4}$$

where $\mathbf{\Sigma}_{r,t}^{s}$ represents the covariance matrix calculated based on the satellite elevation angle and signal-to-noise ratio (SNR) [14].

Unlike our previous work on the loosely-coupled Doppler factor [11], we employed the tightly-coupled Doppler factor in the proposed method. Given the Doppler measurement $(d_{r,t}^{1}, d_{r,t}^{2}, ...)$ of each satellite at an epoch t. The range rate measurement vector $(\mathbf{y}_{r,t}^{d})$ at an epoch t is expressed as follows:

$$\mathbf{y}_{r,t}^{d} = (\lambda d_{r,t}^{1}, \lambda d_{r,t}^{2}, \lambda d_{r,t}^{3}, \dots)^{T} \tag{5}$$

where the λ denotes the carrier wavelength of the satellite signal, the $d_{r,t}^{s}$ represents the Doppler measurement. The expected range rate $rr_{r,t}^{s}$ for satellite s can also be calculated as follows:

$$rr_{r,t}^{s} = \mathbf{e}_{r,t}^{s,LOS}(\mathbf{v}_{t}^{s} - \mathbf{v}_{r,t}) + \frac{\omega_{earth}}{c_{L}}(\mathrm{v}_{t,y}^{s}\mathrm{p}_{r,t,x} + \mathrm{p}_{t,y}^{s}\mathrm{v}_{r,t,x} - \mathrm{p}_{t,x}^{s}\mathrm{v}_{r,t,y} - \mathrm{v}_{t,x}^{s}\mathrm{p}_{r,t,y}) \tag{6}$$

where the variable ω_{earth} denotes the angular velocity of the earth's rotation [15]. The variable c_{L} denotes the speed of light. The variable $\mathbf{e}_{r,t}^{s,LOS}$ denotes the line-of-sight vector connecting the GNSS receiver and the satellite. Based the above equation, the error function of the Doppler factor $\mathbf{e}_{r,t}^{D}$ can be written as follows:

$$||\mathbf{e}_{r,t}^{s,D}||_{\mathbf{\Sigma}_{r,t}^{D}}^{2} = ||\lambda d_{r,t}^{s} - rr_{r,t}^{s}||_{\mathbf{\Sigma}_{r,t}^{D}}^{2} \tag{5}$$

where $\mathbf{\Sigma}_{r,t}^{D}$ denotes the covariance matrix corresponding to the Doppler measurement and calculated with the same method based on satellite elevation angle and SNR [14].

3.2 Constant velocity factor

The constant velocity factor is constructed based on the speed between two consecutive epochs that would not be widely divergent. Hence, we can get the observation model for the velocity $(\mathbf{v}_{r,t})$ is expressed as follows:

$$h_{r,t}^{mm}(\Delta\mathbf{p}_{r,t}, \mathbf{v}_{r,t}, \mathbf{v}_{r,t+1}) = \begin{bmatrix} \Delta p_{r,t,x}/\Delta t - (v_{r,t,x} + p_{r,t+1,x})/2 \\ \Delta p_{r,t,y}/\Delta t - (v_{r,t,y} + p_{r,t+1,y})/2 \\ \Delta p_{r,t,z}/\Delta t - (v_{r,t,z} + p_{r,t+1,z})/2 \end{bmatrix}, \quad (6)$$

where the $\mathbf{v}_{r,t}$ and $\mathbf{v}_{r,t+1}$ denote the velocity at two consecutive epochs with three-dimension in the ECEF frame, respectively. $\Delta p_{r,t,x}$, $\Delta p_{r,t,y}$, $\Delta p_{r,t,z}$ denote the receiver displacement between the t frame and t+1 frame at three dimensions. The variable $\boldsymbol{\omega}_{r,t}^{mm}$ denotes the noise associated with constant motion. The error function of the constant velocity factor could be written as:

$$||\mathbf{e}_{r,t}^{mm}||_{\boldsymbol{\Sigma}_{r,t}^{mm}}^2 = ||h_{r,t}^{mm}(\Delta\mathbf{p}_{r,t}, \mathbf{v}_{r,t}, \mathbf{v}_{r,t+1)}||_{\boldsymbol{\Sigma}_{r,t}^{mm}}^2 \quad (7)$$

where the $\boldsymbol{\Sigma}_{r,t}^{mm}$ is denoted by the covariance matrix and set as the fixed value. NLOS Exclusion and GNSS-RTK Positioning

3.3 Graduated Non-convexity for Outlier Mitigation

This section mainly follows the work in [13]. For complementary, we do the concise present here. The GNC is employed in the system to mitigate the outliers in GNSS measurements. Firstly, the residuals would be calculated and sent to the adaptive weighting estimation after the estimation. Secondly, the weightings for each pseudorange measurement would be estimated by the residuals which is the key part of the outlier mitigation of the proposed method. Finally, the estimated weightings would be used in the FGO in the robust estimation for every given pseudorange. More details about GNC can be found in [13]. For conventional object function for GNSS standalone integration using FGO could be written as:

$$\boldsymbol{\chi}^* = \underset{\boldsymbol{\chi}}{argmin} \sum_{s,t}(||\boldsymbol{e}_{r,t}^D||_{\boldsymbol{\Sigma}_{r,t}^D}^2 + ||\boldsymbol{e}_{r,t}^{mm}||_{\boldsymbol{\Sigma}_{r,t}^{mm}}^2 + ||\boldsymbol{e}_{r,t}^s||_{\boldsymbol{\Sigma}_{r,t}^s}^2) \quad (8)$$

After optimization, we found there is still a long tail in the histogram of the pseudorange residuals, which is mainly caused by the outlier pseudorange measurements. To reduce the impact of the outlier which the non-linear least-square problem is sensitive, we implement the GNC and the updated object function is:

$$\boldsymbol{\chi}^* = \underset{\boldsymbol{\chi},\boldsymbol{\mathcal{W}}}{argmin} \sum_{s,t} ||\boldsymbol{e}_{r,t}^D||_{\boldsymbol{\Sigma}_{r,t}^D}^2 + ||\boldsymbol{e}_{r,t}^{mm}||_{\boldsymbol{\Sigma}_{r,t}^{mm}}^2 + \omega_{t,s}||\boldsymbol{e}_{r,t}^s||_{\boldsymbol{\Sigma}_{r,t}^s}^2 + \emptyset_{\rho_\theta}(\omega_{t,s}) \quad (9)$$

$$\emptyset_{\rho_\theta}(\omega_{t,s}) = \theta\ (c_{GM})^2(\sqrt{\omega_{t,s}} - 1)^2 \quad (10)$$

where the $\omega_{t,s}$ is the weighting for a given pseudorange measurement, the variable $\boldsymbol{\mathcal{W}}$ is a set of weightings of $\omega_{t,s}$. $\emptyset_{\rho_\theta}(\omega_{t,s})$ is the surrogated penalty function [12]. Solving the (9) equals finding the optimal state estimation of the smartphone and the optimal weightings of pseudorange measurements to minimize the summation of the residuals. Fortunately, the $\omega_{t,s}$ could be directly solved as:

$$\omega_{t,s} = \frac{\theta\cdot(c_{GM})^2}{\theta\cdot(c_{GM})^2 + (e_{r,t}^s)^2} \quad (11)$$

where θ is the control parameter and c_{GM} is the parameter for determining the shape of the Geman McClure function.

4. EXPERIMENTAL RESULTS

4.1 Experimental Setup

We collect the dataset in the typical urban canyons located in Shang Hai, and we also use one of the training datasets of Google Decimeter Challenge 2022 in Los Angeles. Fig. 3 shows smartphones used for data collection. Meanwhile, the tested scene is shown on the left-hand side of Fig. 3 which involves tall buildings and even the stadium is challenging for GNSS positioning. In urban canyon 1, a Huawei P40 Pro was used to collect raw GPS/BeiDou measurements at a frequency of 1 Hz. In the training datasets (urban canyon 2), the raw GPS, GLONASS, Beidou, and GALILEO measurements were collected at 1Hz. It should be noticed that the L5 frequency data is also available. In addition, the NovAtel SPAN-CPT, a GNSS (GPS, GLONASS, and Beidou) RTK/INS (fiber-optic gyroscopes, FOG) integrated navigation system was used to provide ground truth of positioning for Shang Hai datasets. The gyro bias in-run stability of the FOG is 1 degree per hour, and its random walk is 0.067 degrees per hour. Google provided the ground truth of Los Angeles. We did not implement the reference station messages in our system.

We analyzed several methods performance in those urban canyons, as shown below. We do the comparison in order to validate that the proposed method have a significant improvement than before. The accuracy is evaluated in the ENU frame by selecting the first point as the reference position.

(a) **WLS [16]:** GNSS positioning is based on the pseudorange using WLS via RTKLIB.
(b) **EKF:** GNSS positioning based on the integration of pseudorange and velocity from Doppler measurements using the EKF estimator.

(c) **FGO-SW**: Real-time sliding window-based GNSS pseudorange/ tightly-coupled Doppler integration using FGO.
(d) **FGO-Batch:** Batch GNSS pseudorange/ tightly-coupled Doppler integration using FGO.
(e) **FGO-GNC-SW:** Real-time sliding window-based GNSS pseudorange/ tightly-coupled Doppler integration using FGO-GNC.
(f) **FGO-GNC-Batch:** Batch GNSS pseudorange/ tightly-coupled Doppler integration using FGO-GNC

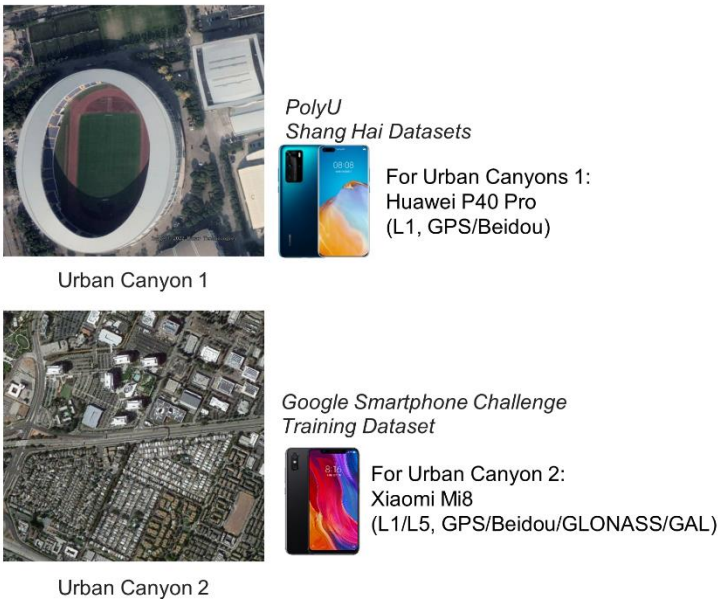

Fig. 3. Illustration of the data collection sensors and tested scenarios.

We analyzed several methods performance in those urban canyons, as shown below. We do the comparison in order to validate that the proposed method have a significant improvement than before. The accuracy is evaluated in the ENU frame by selecting the first point as the reference position.

(g) **WLS [16]:** GNSS positioning is based on the pseudorange using WLS.
(h) **EKF:** GNSS positioning based on the integration of pseudorange and velocity from Doppler measurements using the EKF estimator.
(i) **FGO-SW**: Real-time sliding window-based GNSS pseudorange/ tightly-coupled Doppler integration using FGO.
(j) **FGO-Batch:** Batch GNSS pseudorange/ tightly-coupled Doppler integration using FGO.
(k) **FGO-GNC-SW:** Real-time sliding window-based GNSS pseudorange/ tightly-coupled Doppler integration using FGO-GNC.
(l) **FGO-GNC-Batch:** Batch GNSS pseudorange/ tightly-coupled Doppler integration using FGO-GNC

6.2 Performance Evaluation in Urban Canyon 1

The results of the six methods mentioned above are shown in Table 2. WLS shows the 13.2 meters mean error in this scenario. Compared to the WLS performance, all the FGO-based methods show better performance. Our proposed real-time method, FGO-GNC-SW, can achieve 7.6 meters mean error, which is more accurate than FGO-SW's 8.7 meters mean error. This result proves our previous GNC-aided method is effective in outlier mitigation. Besides the above conclusion, it can also be seen that FGO-GNC-Batch significantly improved over all the other methods with the 7.0 meters mean error.

Table 2. Positioning performance comparison of urban canyon 1.

Method	RMSE (m)	Mean (m)	Max(m)
WLS	18.8	13.2	219.0
EKF	18.8	13.1	117.6
FGO-SW	10.8	8.7	41.0
FGO-Batch	10.1	8.5	39.8
FGO-GNC-SW	9.1	7.6	43.2
FGO-GNC-Batch	8.2	7.0	38.8

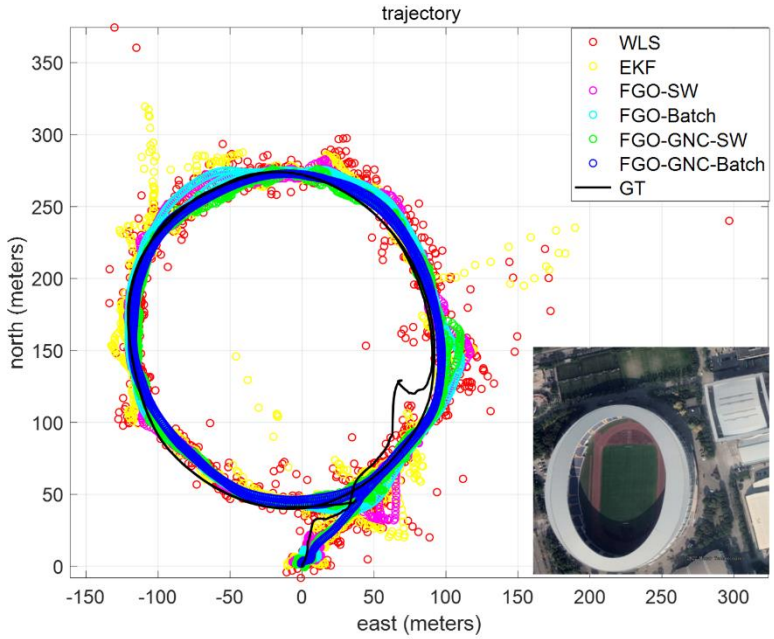

Fig. 4. Trajectories of the evaluated methods. The black curve denotes the ground truth (GT). The red, yellow, magenta, cyan, green, and blue curves denote the solutions from WLS, EKF, FGO-SW, FGO-Batch, FGO-GNC-SW, and FGO-GNC-Batch, respectively.

The trajectories of the evaluated six methods and the ground truth are shown in Fig. 4. This scenario is around the stadium. The positioning errors throughout the experiment are shown in Fig. 5. Clearly, the overall GNC-aided methods have lower errors, in other words, both FGO-GNC-SW and FGO-GNC-Batch exhibit a lower error compared to FGO-SW and FGO-Batch. However, it is also important to note that although GNC-aided FGO has a lower error overall, it should be noted that the error of GNC-aided FGO is larger than that of non-GNC-aided methods in some periods.

In short, the proposed real-time optimization method FGO-GNC-SW can have a better performance than FGO-SW and FGO-Batch, guaranteeing real-time performance. The FGO-GNC-Batch would achieve better performance than FGO-GNC-SW, but it increases time consumption by a higher computational load. We will discuss the relationship between time consumption and window size in section 5.

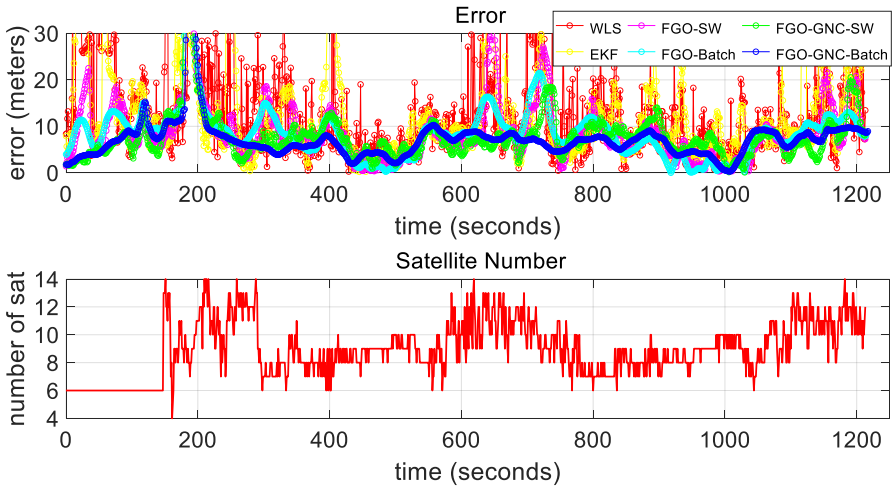

Fig. 5. The top panel shows the errors of the evaluated methods. The red, yellow, magenta, cyan, green, and blue curves denote the solutions from WLS, EKF, FGO-SW, FGO-Batch, FGO-GNC-SW, FGO-GNC-Batch, respectively. The bottom panel shows the number of excluded GNSS NLOS satellites during the experiment.

6.3 Performance Evaluation in Urban Canyon 2

Table 2. Positioning performance comparison of urban canyon 2.

Method	RMSE (m)	Mean (m)	Max(m)
WLS	12.9	11.0	6.9
EKF	32.0	26.1	26.3
FGO-SW	5.6	4.8	2.7
FGO-Batch	4.2	3.3	2.5
FGO-GNC-SW	4.8	4.0	2.6
FGO-GNC-Batch	4.0	3.2	2.3

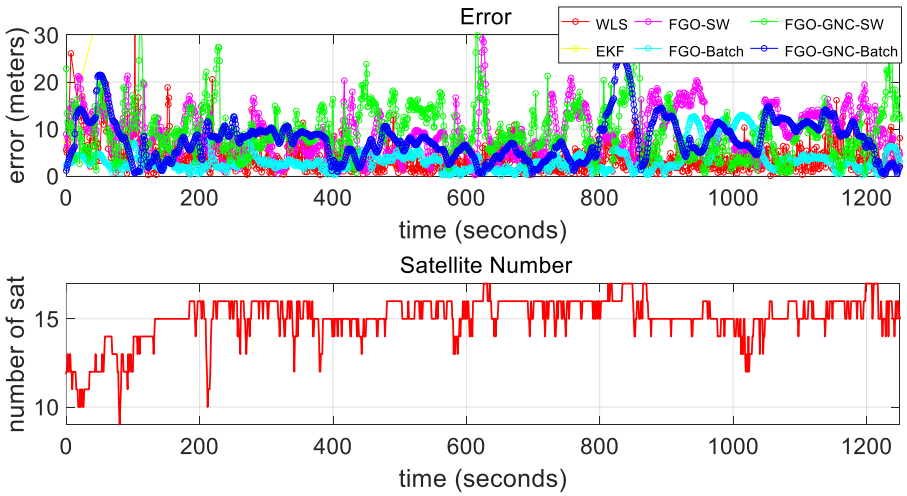

Fig. 6. The top panel shows the errors of the evaluated methods. The red, yellow, magenta, cyan, green, and blue curves denote the solutions from WLS, EKF, FGO-SW, FGO-Batch, FGO-GNC-SW,FGO-GNC-Batch, respectively. The bottom panel shows the number of excluded GNSS NLOS satellites during the experiment.

Google Decimeter Challenge release many datasets for training this year. We use the MTV dataset to validate our proposed method. The Table 3 shows the positioning performance of all the methods in urban canyon 2. There are the similar conclusion as the urban canyon 1's. The FGO-GNC-SW could achieve 4.0 meters mean error compared to the 4.8 meters mean error of FGO-SW. Fig. 6 shows the positioning errors of all six methods in urban canyon 2. Like the conclusion of the experiment in urban canyon 1, GNC-aided FGO could have better overall performance, but in some cases aiding GNC would decrease the positioning error.

5. DISCUSSION ABOUT THE TIME CONSUMPTION

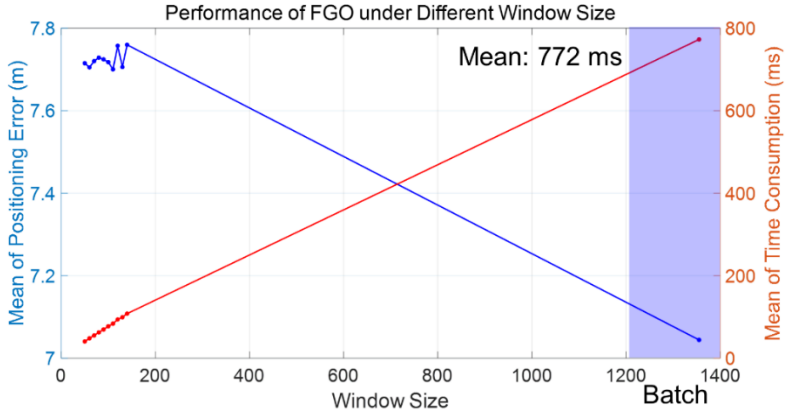

Fig. 7. The relationship between time consumption and positioning error under different window sizes of the FGO. The blue curve denotes the positioning error in different window sizes. The red curve represents the time consumption in different window sizes.

Real-time performance is one of the most vital metrics for evaluating the method's feasibility. Fig 7 shows the relationship between positioning error and consumption under different window sizes.

From Fig. 7, we can see that the overall time consumption also increases when the sliding window increases. The time consumption reaches a maximum of 772 ms when the FGO-GNC is under batch mode, and although the computational load is increased, the average value of the localization error is effectively reduced. In FGO-GNC-SW, the average values of time loss are all below 0.2 s, while the loss of positioning accuracy is acceptable at around 7.7m.

6. CONCLUSIONS AND FUTURE WORK

FGO has shown its accuracy and robustness in urban canyons [17]. However, there are still severe signal reflections and blockage in typical urban canyons, leading to smartphones receiving many outliers of GNSS measurements. Moreover, the non-linear least-square is sensitive to gross outlier measurements. So we implement the GNC for outlier mitigation in GNSS positioning and achieve 7.0 meters positioning error in urban canyon 1. Furthermore, to implement our method in the smartphone, we proposed a real-time sliding window-based GNSS pseudorange/ Doppler positioning method using FGO-GNC. Within an acceptable loss of accuracy, FGO-GNC-SW has significantly reduced the computational load by using sliding windows, with an average solution time of fewer than 0.5 seconds per epoch,

According to the results, we still find some degradation of the FGO-GNC-Batch compared to the FGO-Batch in some periods. This phenomenon may be caused by strict outlier mitigation, which would de-weighting some health measurements. The GNC's drawback is that the control parameter should be adjusted case by case. In the future, we will do the adaptive GNC which means the control parameters could be adaptive to avoid the de-weighting of the reliable measurements. By using the adaptive GNC, the time consumption may be lower with more accurate positioning performance.

Acknowledgment
This research is supported by the University Grants Committee of Hong Kong under the scheme Research Impact Fund on the project R5009-21 "Reliable Multiagent Collaborative Global Navigation Satellite System Positioning for Intelligent Transportation Systems.

REFERENCES

[1] T. Suzuki, "First place award winner of the smartphone decimeter challenge: global optimization of position and velocity by factor graph optimization," in *Proceedings of the 34th International Technical Meeting of the Satellite Division of The Institute of Navigation (ION GNSS+ 2021)*, 2021, pp. 2974-2985.

[2] T. Tang, Q. Hu, Y. Xiang, S. Lye, and W. Yu, "High Precision GNSS Positioning on Smartphones Challenge-On Smartphone-Based Wide Area High Precision Positioning using SSR," in *Proceedings of the 34th International Technical Meeting of the Satellite Division of The Institute of Navigation (ION GNSS+ 2021)*, 2021, pp. 3059-3067.

[3] F. Zangenehnejad and Y. Gao, "Application of UofC Model Based Multi-GNSS PPP to Smartphones GNSS Positioning," in *Proceedings of the 34th International Technical Meeting of the Satellite Division of the Institute of Navigation (ION GNSS+ 2021)*, 2021, pp. 2986-3003.

[4] F. Dellaert and M. Kaess, "Factor graphs for robot perception," 2017.

[5] N. Sünderhauf and P. Protzel, "Switchable constraints for robust pose graph SLAM," in *2012 IEEE/RSJ International Conference on Intelligent Robots and Systems*, 2012: IEEE, pp. 1879-1884.

[6] C. Kilic, S. Das, E. Gutierrez, R. Watson, and J. Gross, "ZUPT Aided GNSS Factor Graph with Inertial Navigation Integration for Wheeled Robots," in *Proceedings of the 34th International Technical Meeting of the Satellite Division of The Institute of Navigation (ION GNSS+ 2021)*, 2021, pp. 3285-3293.

[7] R. M. Watson and J. N. Gross, "Robust navigation in GNSS degraded environment using graph optimization," in *Proceedings of the 30th international technical meeting of the satellite division of the institute of navigation (ION GNSS+ 2017)*, 2017, pp. 2906-2918.

[8] W. Wen, X. Bai, Y. C. Kan, and L.-T. Hsu, "Tightly coupled GNSS/INS integration via factor graph and aided by fish-eye camera," *IEEE Transactions on Vehicular Technology*, vol. 68, no. 11, pp. 10651-10662, 2019.

[9] W. Wen, T. Pfeifer, X. Bai, and L.-T. Hsu, "Factor graph optimization for GNSS/INS integration: A comparison with the extended Kalman filter," *NAVIGATION, Journal of the Institute of Navigation*, vol. 68, no. 2, pp. 315-331, 2021.

[10] S. Das, R. Watson, and J. Gross, "Review of Factor Graphs for Robust GNSS Applications," *arXiv preprint arXiv:2112.07794*, 2021.

[11] W. Wen and L.-T. Hsu, "Towards robust GNSS positioning and Real-time kinematic using factor graph optimization," in *2021 IEEE International Conference on Robotics and Automation (ICRA)*, 2021: IEEE, pp. 5884-5890.

[12] H. Yang, P. Antonante, V. Tzoumas, and L. Carlone, "Graduated non-convexity for robust spatial perception: From non-minimal solvers to global outlier rejection," *IEEE Robotics and Automation Letters*, vol. 5, no. 2, pp. 1127-1134, 2020.
[13] W. Wen, G. Zhang, and L.-T. Hsu, "GNSS outlier mitigation via graduated non-convexity factor graph optimization," *IEEE Transactions on Vehicular Technology*, vol. 71, no. 1, pp. 297-310, 2021.
[14] A. M. Herrera, H. F. Suhandri, E. Realini, M. Reguzzoni, and M. de Lacy, "goGPS: open-source MATLAB software," *GPS solutions*, vol. 20, no. 3, pp. 595-603, 2016.
[15] T. Takasu and A. Yasuda, "Development of the low-cost RTK-GPS receiver with an open source program package RTKLIB," in *International symposium on GPS/GNSS*, 2009: International Convention Center Jeju Korea, pp. 4-6.
[16] T. Takasu and A. Yasuda, "Development of the low-cost RTK-GPS receiver with an open source program package RTKLIB," in *International symposium on GPS/GNSS*, 2009, vol. 1: International Convention Center Jeju Korea.
[17] W. Wen, Y. C. Kan, and L.-T. Hsu, "Performance comparison of GNSS/INS integrations based on EKF and factor graph optimization," in *Proceedings of the 32nd International Technical Meeting of the Satellite Division of The Institute of Navigation (ION GNSS+ 2019)*, 2019, pp. 3019-3032.